CASES: A Smart, Compact GPS Software Receiver for Space Weather Monitoring

Brady W. O'Hanlon, Mark L. Psiaki, Steven Powell, *Cornell University, Ithaca NY*
Jahshan A. Bhatti, Todd E. Humphreys, *The University of Texas, Austin TX*
Geoff Crowley, Gary S. Bust, *ASTRA, Boulder CO*

BIOGRAPHY

Brady W. O'Hanlon is a graduate student in the School of Electrical and Computer Engineering at Cornell University. He received a B.S. in Electrical and Computer Engineering from Cornell University in 2007. His interests are in the areas of GNSS technology and applications, GNSS security, and GNSS as a tool for space weather research.

Mark L. Psiaki is a Professor in the Sibley School of Mechanical and Aerospace Engineering. He received a B.A. in Physics and M.A. and Ph.D. degrees in Mechanical and Aerospace Engineering from Princeton University. His research interests are in the areas of GNSS technology and applications, spacecraft attitude and orbit determination, and general estimation, filtering, and detection.

Steven Powell is a Senior Engineer with the GPS and Ionospheric Studies Research Group in the Department of Electrical and Computer Engineering at Cornell University. He has been involved with the design, fabrication, testing, and launch activities of many scientific experiments that have flown on high altitude balloons, sounding rockets, and small satellites. He has designed ground-based and space-based custom GPS receiving systems primarily for scientific applications. He has M.S. and B.S. degrees in Electrical Engineering from Cornell University.

Jahshan A. Bhatti is pursuing a Ph.D. in the Department of Aerospace Engineering and Engineering Mechanics at the University of Texas at Austin, where he also received his M.S. and B.S. He is a member of the UT Radionavigation Laboratory. His research interests are in the development of small satellites, software-defined radio applications, space weather, and GNSS security and integrity.

Todd E. Humphreys is an assistant professor in the department of Aerospace Engineering and Engineering Mechanics at the University of Texas at Austin and Director of the UT Radionavigation Laboratory. He received a B.S. and M.S. in Electrical and Computer Engineering from Utah State University and a Ph.D. in

Aerospace Engineering from Cornell University. His research interests are in estimation and filtering, GNSS technology, GNSS-based study of the ionosphere and neutral atmosphere, and GNSS security and integrity.

Geoff Crowley is President and Chief Scientist of Atmospheric & Space Technology Research Associates (ASTRA) LLC. He is well known for research on space weather, ionospheric variability and high latitude processes, including modeling of the global ionosphere-thermosphere system in response to geomagnetic storms. He has authored or co-authored over 90 refereed papers. He is PI of the DICE Cubesat mission, and leads several technology development projects at ASTRA including the development of software-based receivers, HF sounders, and satellite avionics. He is a founding member and serves on the Executive Council of the American Commercial Space Weather Association (ACSWA). He has a B.Sc. (Hons) in Physics from Durham University, UK, and a Ph.D. in Ionospheric Physics from the University of Leicester, UK.

Gary Bust received his Ph.D. in Physics in 1989 from the University of Texas at Austin, and is currently Senior Research Scientist at Atmospheric and Space Technology Research Associates. He has worked in the areas of ionospheric tomographic imaging, data assimilation and the application of space-based observations to ionospheric remote sensing for over 17 years. Dr. Bust has authored over 30 papers on ionospheric imaging and has continued development of the ionospheric imaging algorithm: "ionospheric data assimilation four-dimensional" (IDA4D) over the last 17 years.

ABSTRACT

A real-time software-defined GPS receiver for the L1 C/A and L2C codes has been developed as a low-cost space weather instrument for monitoring ionospheric scintillation and total electron content. The so-called CASES receiver implements several novel processing techniques not previously published that make it well suited for space weather monitoring: (A) a differencing technique for eliminating local clock effects, (B) an advanced triggering mechanism for determining the onset

of scintillation, (C) data buffering to permit observation of the prelude to scintillation, and (D) data-bit prediction and wipe-off for robust tracking. The receiver has been tested in a variety of benign and adverse signal conditions (e.g., severe ionospheric scintillation, both real and simulated); the results are presented here. The custom hardware platform on which the software runs is compact while remaining flexible and extensible. The CASES platform consists of a digital signal processor, an ARM microcontroller, and a custom-built narrow-band dual-frequency front end. Because the receiver is software-defined, it can be remotely reprogrammed via the internet or another communications link.

I. INTRODUCTION

CASES (Connected Autonomous Space Environment Sensor) was designed to facilitate ionospheric study[1]. Study of the Earth's ionosphere is a particularly difficult proposition due to its location, spanning from one hundred kilometers or so to greater than one thousand kilometers above the Earth's surface. As the signals from GPS satellites traverse this region and are changed by disturbances therein, they provide a unique tool for studying the structure and variations of the ionosphere. GPS signals are changed in two ways of interest: refraction due to the presence of charged particles in the ray path, and diffraction due to the occasionally irregular densities of those charged particles. The path-integrated number of electrons (total electron content, or TEC) can be observed by comparing observations on multiple frequencies. The effects of density irregularities manifest as rapid fluctuations of signal amplitude and/or phase (ionospheric scintillation). GPS receivers have been used to study both of these effects for many years[2]. The CASES receiver differs from typical GNSS receivers in two key ways: it has been specially designed to measure TEC and scintillation parameters, and special features have been implemented that allow it to operate robustly in the presence of vigorous ionospheric scintillation. The estimation of TEC will be lightly treated here, as scintillation provides a much more challenging signal environment than any observed TEC fluctuations, and the measurements needed to estimate TEC are produced in the course of standard receiver operation (e.g., code and carrier phase measurements). Signal variations due to tropospheric effects are not addressed here.

Section II of this paper contains a description of the CASES hardware platform, the available peripherals, and the performance specifications. Section III describes the various novel processing techniques implemented by the receiver. Section IV contains an analysis of the receiver performance under various signal conditions, and Section V contains conclusions. CASES is the result of development effort between Cornell University, the University of Texas at Austin, and ASTRA[3,4].

II. HARDWARE PLATFORM

The CASES receiver was designed with the goal of providing a capable platform with many peripheral options while remaining inexpensive, relatively small, and power-efficient. The final configuration has three main components: a custom-built dual-frequency front end, a digital signal processor board, and a "single board computer" featuring an ARM microcontroller. A block diagram of the receiver hardware is shown in Fig. 1., and a photograph of the receiver in two different configurations is shown in Fig. 2.
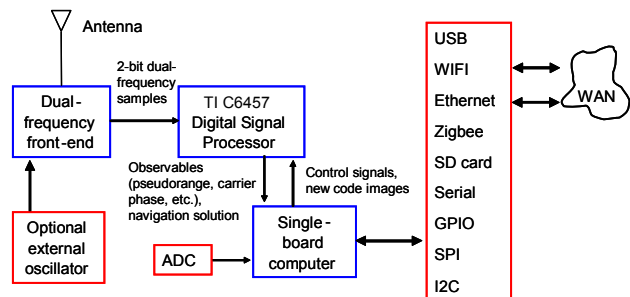

Fig. 1 Receiver Hardware Block Diagram

Fig. 2 CASES in two different form-factors

The front-end performs automatic gain-controlled amplification, filtering, mixing to intermediate frequency, and sampling. The front-end has a relatively narrow bandwidth of 2.4 MHz, and produces 2-bit samples at 5.7 MSamples/second. As it is a dual-frequency front-end, it produces one set of 2-bit samples for each of the GPS L1 and L2 frequencies. An on-board temperature-compensated crystal oscillator (TCXO) is the frequency reference for both frequencies, and both signals are sampled synchronously. Although the use of a TCXO introduces non-negligible variations in measured carrier phase[5], a method to remove this error has been implemented, as discussed in Section III. The front-end can provide a selectable 5 volt DC bias on the antenna input for powering active antennas, and has an optional input for connecting an external 10 MHz frequency

reference, with termination of 50 or 1000 Ohms. The board consumes approximately 360 milliamps at 5 volts, excluding any power required by a connected active antenna.

CASES is a software-defined receiver, with all processing downstream of the front end performed on a general-purpose digital signal processor. A second custom-designed board houses a Texas Instruments C6457 digital signal processor (DSP). The processor runs at a 1 GHz clock speed, has 2 MB of on-chip RAM, 128 MB of off-chip RAM, and 4MB of non-volatile flash memory. The so-called DSP board performs all acquisition and tracking functions, as well as computation of the navigation solution and various observables such as pseudorange, beat carrier phase, and Doppler shift. The board outputs in-phase and quadrature accumulations, beat carrier phase, and timestamps at up to 100 Hz, and all other data at 10 Hz or less. Processor utilization while tracking 12 GPS L1 C/A code channels and 4 GPS L2CL channels as well as computing the navigation solution, performing continuous background signal acquisition, and all other overhead is roughly 75%. The DSP board consumes approximately 580 milliamps at 5 volts.

The third main receiver component is a "single-board computer" (SBC) running the GNU/Linux operating system. The so-called SBC features an ARM AT91SAM9260 microcontroller with a host of available peripherals. This board features 32 MB of RAM and 128 MB of flash memory for the file system. Available peripherals include Ethernet, serial peripheral interface, a secure digital card reader, universal serial bus, ZigBee, Wi-Fi, a 10-bit analog-to-digital converter, and general-purpose I/O pins. Communication is typically done via RS232 serial port, Ethernet, or Wi-Fi. The SBC runs a network-connected server program that allows remote monitoring, data logging, and uploading of new code images or configuration files. Additionally, it runs a secure shell server to allow remote log-in for additional operations not provided by the server program. The SBC consumes approximately 260 milliamps at 5 volts.

III. Novel Software Processing Techniques

Density irregularities in ionospheric plasma can induce rapid fluctuations in the phase and/or amplitude of GPS signals, which can cause the receiver to lose signal lock[2,6]. This problem is even more pronounced for GPS L2P(Y) signals in receivers that employ codeless or semi-codeless tracking techniques, which are more prone to losing lock on the signal due to various losses introduced by the processing[7], and are not well suited for measuring phase scintillation on L2 due to the low tracking loop bandwidth they typically employ[6]. A quantitative relationship between scintillation effects on multiple frequencies is not well understood, though it has long been known that the correlation between multiple frequencies is inversely related to the scintillation intensity (see Fig. 1 of Ref. 8).

Thus, a dual-frequency receiver is desirable both for estimating TEC and for estimating ionospheric scintillation parameters at disparate frequencies, as multiple-frequency scintillation parameter estimation provides non-redundant information. Several techniques have been implemented to make the receiver particularly well suited for scintillation monitoring.

A. Removal of local clock effects

Ionospheric scintillation severity is typically characterized by two parameters: S_4, the normalized signal amplitude standard deviation, and σ_φ, the carrier phase standard deviation[9]. Unfortunately, the phase noise introduced by a receiver's TCXO (such as the one used in CASES) is spectrally similar to the phase fluctuations from ionospheric scintillation (see Fig. 2 in Ref. 5). To prevent local clock variations from contaminating measured scintillation parameters, the CASES receiver pre-processes the carrier phase time histories to remove common-mode clock effects, prior to estimating the scintillation parameters. The key idea in this algorithm is that the TCXO-induced phase noise can be estimated by observing phase fluctuations from a signal that is known to be free of ionosphere-induced phase variations[10]. Just how one knows that a signal is free of these fluctuations prior to the calculation of scintillation parameters whose validity depends on this assumption is a bit of a chicken-and-egg conundrum, but it is readily resolvable, as described in subsection B below. For now, let it be assumed that a suitable reference signal free of ionospheric scintillation has been identified.

The clock effect removal algorithm starts by modeling the beat carrier phase measurements from the nth tracking channel as

$$\phi_n = \phi_{n-geom} + \phi_{clk} + \phi_{n-scint} + n_n \qquad (1)$$

Where ϕ_{n-geom} is the phase component due to satellite geometry, ϕ_{clk} is the phase component due to oscillator noise, $\phi_{n-scint}$ is the phase component due to ionospheric effects, and n is other noise sources (e.g., thermal noise, satellite oscillator noise). Assume that a reference channel free of ionospheric effects has been identified. The phase of the reference channel is modeled as

$$\phi_{ref} = \phi_{ref-geom} + \phi_{clk} + n_{ref} \qquad (2)$$

where the same notation applies as previously, but for the reference channel rather than the nth tracking channel. The difference of these carrier phases is taken, creating a combined carrier phase measurement given by

$$\widetilde{\phi}_n = \phi_n - \phi_{ref}$$
$$= \phi_{n-geom} - \phi_{ref-geom} + \phi_{n-scint} + n_n - n_{ref} \qquad (3)$$

This new phase measurement now contains the combination of the geometric effects for the two channels,

the combination of the noise on the two channels, and the phase fluctuations due to scintillation on channel *n*.

In the next processing step, the differential phase due to geometric effects $\phi_{n-geom} - \phi_{ref-geom}$ is removed. Over time intervals up to 100 seconds, and for stationary GPS receivers, $\phi_{n-geom} - \phi_{ref-geom}$ can be accurately modeled as a 3rd order polynomial. It can then be removed by subtracting a 3rd order polynomial fit to $\tilde{\phi}$ over a 100 second interval. This procedure removes the $\phi_{n-geom} - \phi_{ref-geom}$ component while leaving $\phi_{n-scint}$ unaffected at the frequencies of interest (greater than about 0.2 Hz). The resulting phase after removal of differential geometry terms is modeled as $\tilde{\phi}_{nf} = \phi_{n-scint} + n_n - n_{ref}$. Thus, the phase scintillation on channel *n* is isolated from local clock and satellite motion effects. It should be noted, however, that $\tilde{\phi}_{nf}$ is a filtered version of the phase scintillation effects on channel *n*. Given that vigorous phase scintillation often contains substantial power well beyond the bandwidth of a typical phase tracking loop (e.g., beyond 10 Hz)[11], high-frequency scintillation effects are not present in $\tilde{\phi}_{nf}$. To recover the high-frequency variations induced by scintillation – up to the pre-detection bandwidth $B_{pd} = 1/T_a$, where T_a is the correlation accumulation interval – the instantaneous phase angle of the in-phase and quadrature accumulations $\phi_{IQn} = atan2(Q \cdot d, I \cdot d)$ is added to $\tilde{\phi}_{nf}$

$$\tilde{\phi}_{npd} = \tilde{\phi}_{nf} + \phi_{IQn} \qquad (4)$$

Here, *d* is the +/-1 valued navigation data bit that was in effect over the interval corresponding to I and Q. The quantity $\tilde{\phi}_{npd}$ includes all scintillation frequencies up to the pre-detection bandwidth. For typical T_a=0.02s, B_{pd} = 50 Hz, which is sufficient to capture even vigorous phase scintillation.
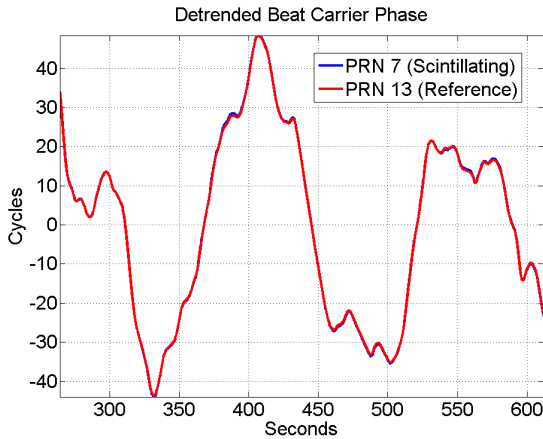

Fig. 3 De-trended beat carrier phase for two satellites

Alternatively, the complex channel response function[11] *z(t)* is produced simply by rotating the vector defined by the I and Q accumulation values by the phase $\tilde{\phi}_{nf}$.

The penalty paid for adding ϕ_{IQn} to $\tilde{\phi}_{nf}$ is, of course, that ϕ_{IQn} includes high-frequency noise in addition to possible high-frequency scintillation. Despite this, $\tilde{\phi}_{npd}$ is a useful new quantity for study of phase scintillation because it is free of local clock, satellite geometry, and phase tracking loop effects.
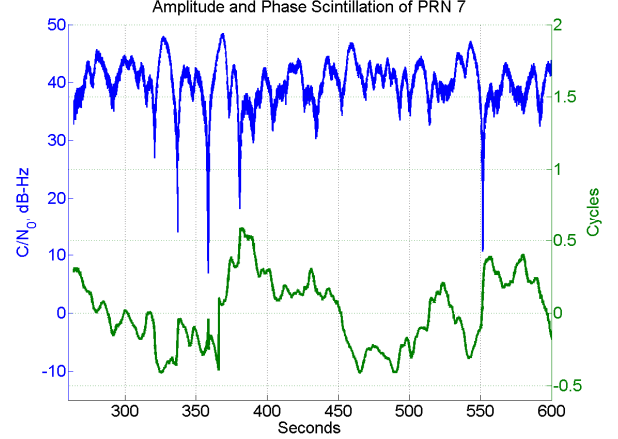

Fig. 4 Amplitude and phase scintillation of a GPS signal

To illustrate the effectiveness of phase pre-processing techniques, consider Figs. 3 and 4. Fig. 3 shows data gathered by the authors during a scintillation campaign at the Jicamarca Radio Observatory near Lima, Peru, in March of 2011. The red signal was the reference channel, and the blue signal (barely visible underneath the red trace) was strongly scintillating.

What is shown is simply the beat carrier phase of the two signals after fitting and removal of a third order polynomial to eliminate geometric effects. The two lines are virtually indistinguishable, indicating that the majority of variation is due to clock effects. Fig. 4 shows the carrier phase (in green) of this same scintillating signal, after removal of local clock effects and de-trending of the phase measurement. The signal amplitude is shown in blue. This plot shows easily recognizable "canonical fades"[11]: abrupt half-cycle phase shifts coincident with deep amplitude fades.
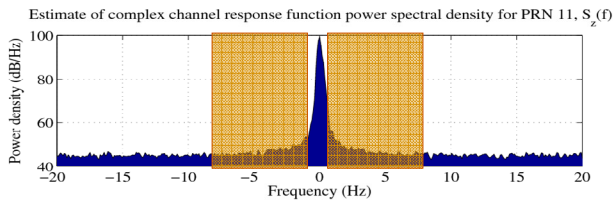
B. An advanced triggering mechanism for determining the onset of scintillation

Due to the high data rates involved when logging data for scintillation study, it is desirable to have a reliable indicator for when signals are experiencing scintillation to avoid recording large amounts of uninteresting data. To put this in perspective, suppose a single "scintillation record" (e.g., amplitude, phase, and time stamp) takes 24

bytes to store. Recording these data for 24 individuals channels at 100 Hz requires about 5 GB per day. Processing this amount of data is prohibitive and even simply storing it quickly becomes onerous. Historically, receivers have used the aforementioned S_4 or σ_φ as triggering mechanisms: when one of these parameters exceeds some preset threshold, high data rate logging is begun. However, from a modeling standpoint it is desirable to have a single parameter that triggers the logging rather than some combination of two parameters. Further, σ_φ has been shown to be an unreliable indicator of scintillation intensity[12,13]. These requirements led to the development of a spectrum-based triggering mechanism; this accounts for both amplitude and phase fluctuations, and a single triggering statistic can be computed by considering the ratio of power in a particular band to the total amount of power measured. This metric has been termed the "scintillation power ratio," or SPR. It should be noted that as this statistic includes the 100 Hz amplitude and phase data, the bandwidth is determined by the pre-detection bandwidth rather than the PLL bandwidth.

To compute the scintillation power ratio, the following steps are taken, using a 100 second window of data:

1. Remove local clock effects from carrier phase measurements and detrend, as in section A, above.
2. Rotate the vector defined by the in-phase and quadrature accumulations by the phase from step 1. This results in a complex time history of the signal, with variations due only to ionospheric effects and noise terms.
3. Apply a windowing function (CASES uses a Hann window).
4. Take the FFT of the result.
5. Compute the ratio of the power in a particular frequency band to the total power.

Fig. 5 Power spectrum of the complex channel response functions of a scintillating signal. Frequency bands used for the scintillation power ratio are shown in orange.

The frequency band used for triggering is set to ±(0.2-8) Hz, though the user can change this. Fig. 5 shows the complex channel response function power spectral density (i.e., the result produced after step 4 of the above algorithm) for a GPS signal that was experiencing scintillation. There is a large DC component to this signal due to the direct component of the channel response function[13]. The frequency bands used in the SPR calculation are highlighted in this figure, and were chosen

by examining a large amount of actual equatorial scintillation, as well as existing literature that has done similar examinations[5,9,11]. Preliminary results from using CASES have shown that these frequency bands are also appropriate for studying high-latitude scintillation.

An elevation mask is used to exclude satellites below a particular elevation from the calculation in order to minimize contributions from multipath errors. The frequency band used in the SPR calculation can be set by the user to any value using a configuration file. Similarly, the user can select a different window length, triggering threshold, elevation mask angle, and frequency resolution for the FFT.

As promised, the issue of reference channel selection will now be revisited. To locate a channel that is free of ionospheric effects, the SPR is calculated using every possible pair of channels that are tracking the same signal type (e.g, GPS L1 C/A) with one of the channels acting as reference. The pair of channels that produce the lowest SPR (and has an SPR below some much more stringent threshold than the threshold used for triggering) are both declared reference channels. The SPR for this pair of channels is re-checked each time SPR is calculated to make sure it remains below the reference power threshold. If it exceeds that threshold, it is assumed that one or both of the reference channels are scintillating, and a new set of reference channels is searched for.

C. Data buffering

As discussed in subsection B above, triggering of high rate data logging is used to effectively filter out "uninteresting" data, and minimize storage and processing requirements. This triggering method operates on batches of data 100 seconds in length for CASES, but window lengths of 60 seconds are common[10]. The result of this is that by the time high-rate data is triggered, some time has elapsed since the onset of scintillation, and in the worst case an entire window period has passed. As this receiver was designed to advance the study of scintillation (among other goals), it seems prudent to provide the greatest amount of data from these events as is possible. Further, studying the onset of these events may prove critical to understanding the underlying atmospheric dynamics. With that in mind, a buffering scheme was implemented whereby data from all satellites is stored in a circular buffer (i.e., first in, first out) for 120 seconds. If a scintillation event is detected, the receiver outputs the data in the buffer for the scintillating signal. This is illustrated in Fig. 6. The data in Fig. 6 are actual (mild) amplitude scintillation gathered by the authors during a campaign in March, 2011 in Lima, Peru. Suppose the triggering mechanism used the window indicated by the highlighted region for detection. In most receivers, if the indicated amplitude fade caused the detection statistic to trigger high-rate logging, it would not begin until the end of the window (as data from the entire window are used in calculating the statistic). In so doing, potentially valuable

data are thrown away. By buffering data, CASES is able to log from the beginning of the plot, two minutes prior to the event that indicated scintillation was occurring.
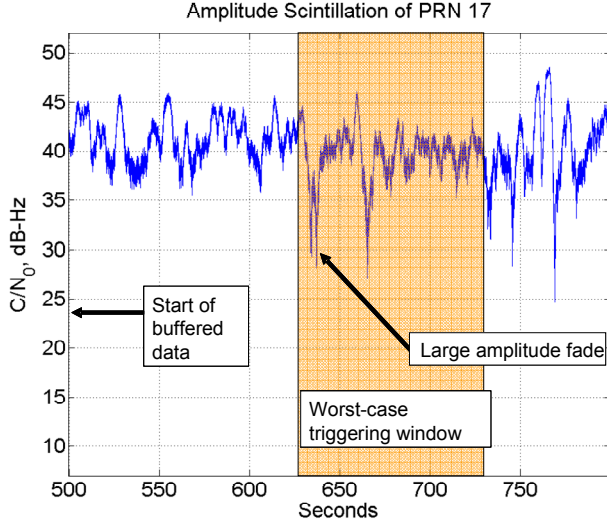

Fig. 6 Illustration of the benefits of data buffering.

D. Data bit prediction

Scintillation-induced phase variations are particularly troublesome for the carrier tracking loops of GPS receivers, and present as a variety of phenomena including cycle-slipping and frequency unlock[6]. For a receiver designed to study scintillation effects, it behooves the designer to make the receiver as resistant to these effects as possible. GPS receivers generally operate with Costas-type PLL discriminators due to the modulation of the signal by the unknown 50 Hz data bit stream. This induces a loss of loop SNR known as squaring loss[14]. Carrier tracking performance can be improved with judicious choices for the pre-detection interval, the loop bandwidth, and the loop discriminator[13]. CASES employs a 3rd order PLL with a decision-directed arctangent discriminator, a 7.5 Hz loop bandwidth, and a 10 millisecond pre-detection interval.

If the data bits are known a priori, a full-cycle (i.e., non-squaring) type PLL can be used, further improving tracking. This is particularly effective when in the presence of scintillation due to the aforementioned "canonical fades" that occur during scintillation, which manifest as half-cycle phase jumps. If the data bits are known, these phase jumps can be rightly measured as scintillation-induced variations rather than part of the signal. In the case of GPS, the 12.5 minute navigation message conveyed by the data bits changes quite infrequently (on even-numbered hours when the ephemeris data are updated or roughly daily in the case of almanac data). CASES records a library of observed data bits when the carrier-to-noise ratio is above a preset threshold, then uses these recorded data bits in the PLL if the carrier-to-noise ratio drops below that threshold (a

possible indicator of scintillation). This data bit library also re-computes the time of week and parity data as required (as these are continually changing in a known manner), and monitors for possible ephemeris or almanac data updates. Results from testing of the efficacy of the data-bit prediction algorithm are presented in Section IV. Note that there are small windows of time when the data bit library is unavailable, namely after an ephemeris or almanac data update, though the library makes it known that the bits are unavailable until the new data are recorded.

The L2 civil long signal is used when tracking on the GPS L2 frequency as this signal has no data bit modulation, thereby making it more robust to scintillation for the same reasons as above.

IV. RECEIVER PERFORMANCE ANALYSIS

The receiver has been run using both real and simulated data in an effort both to confirm the operational advantages provided by the novel algorithms implemented herein, and to get a measure of the precision with which it can produce the standard observables such as phase and pseudorange.

A. Measurement Precision

The precision with which pseudorange can be measured is of particular importance as this impacts the accuracy of TEC estimates made using those measurements. The errors in carrier phase measurements are typically two orders of magnitude smaller than those for pseudorange[14].
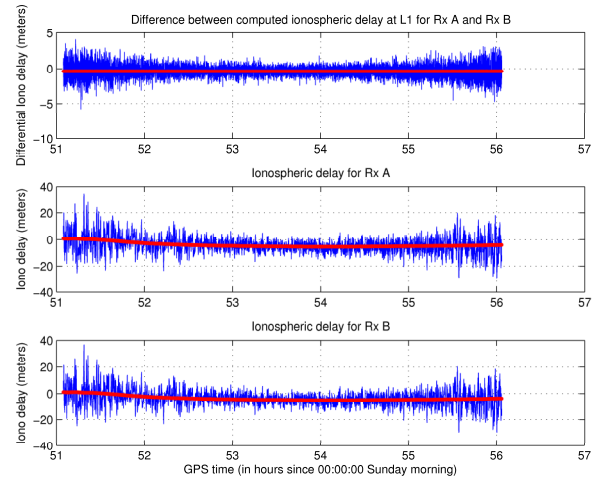

Fig. 7 Single-receiver dual frequency code and carrier phase ionospheric delay at L1 (bottom two panels) and inter-receiver ionospheric delay difference (top panel). The receivers used a common antenna.

To estimate the precision with which CASES can measure pseudorange, two receivers were connected to the same antenna, and TEC was computed using both pseudorange and carrier phase (for an entire satellite pass, about 5 hours). Fig. 7 illustrates this, with the pseudorange-

derived value shown in blue, and carrier-phase-derived value shown in red.

The results for the two receivers are shown in the bottom two panels, while the difference of the results is shown in the top panel. The errors in the top panel are due only to receiver thermal noise, as oscillator effects are removed by creating the differences shown in the bottom two panels, and multipath effects are eliminated in the inter-receiver difference. The minimum RMS noise in the top panel is 0.5 meters, which implies an RMS error for a single receiver of about 0.35 meters. This is the fundamental precision with which CASES can measure pseudorange on L1. Since the L2 civilian signal is weaker than the L1 C/A signal, and the receiver tracks only the civil long code on the L2 frequency, the L2 pseudorange measurements will be slightly worse than this.

Multipath errors can contribute as much as 5 meters (RMS) to pseudorange measurements[15]. As CASES uses a narrow-bandwidth front-end, many advanced multipath mitigation techniques are unsuitable. One approach that is feasible is to tune the delay lock loop early-minus-late correlator spacing, which can result in better multipath rejection at the cost of tracking precision[16]. After testing, a value of 0.6 chips has been determined as optimal for the current receiver, and a (carrier aided) delay lock loop bandwidth of 0.1 Hz is used. The precision of CASES in the presence of multipath after tuning these parameters is
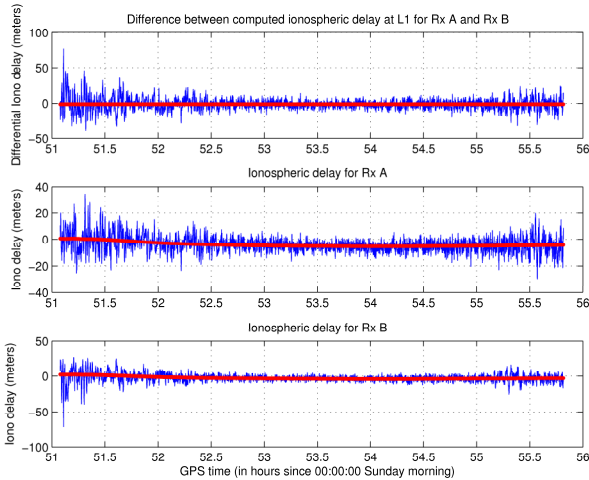

Fig. 8 Single-receiver dual frequency code and carrier phase ionospheric delay at L1 (bottom two panels) and inter-receiver ionospheric delay difference (top panel). The receivers used independent antennas.

shown in Fig. 8. Again, pseudorange is shown in blue, carrier phase in red. In this plot, the two receivers (bottom two panels), are connected to different antennas. In this test, Rx A was in a good multipath environment, while Rx B was in a poor multipath environment (note the differing vertical scales). The RMS pseudorange error

here for a single receiver (when the satellite was at high elevation) is 2.7 meters, but it should be noted that this is merely illustrating a typical value for pseudorange errors in the presence of multipath; the particular antenna used and the multipath environment are all significant factors here and any particular case could differ significantly.

B. Scintillation Robustness

Testing of the data bit prediction algorithm has shown that CASES is highly resistant to half-cycle phase jumps while experiencing ionospheric scintillation. To conduct this test a scintillation scenario was generated using the Cornell Scintillation Model[17] on a Spirent GSS7700 GPS signal Simulator. The simulation parameters were expected C/N_0 = 43 dB-Hz, S_4=0.8, τ_0=0.8 s. The resultant signal was then tracked using CASES, and the measured phase history was subtracted from the true phase history recorded by the signal simulator. The CASES tracking was done in a post-processing mode after recording the data from the Spirent to ensure that exactly the same data was used for the comparison. The results of this test are shown in Figs. 9 and 10.
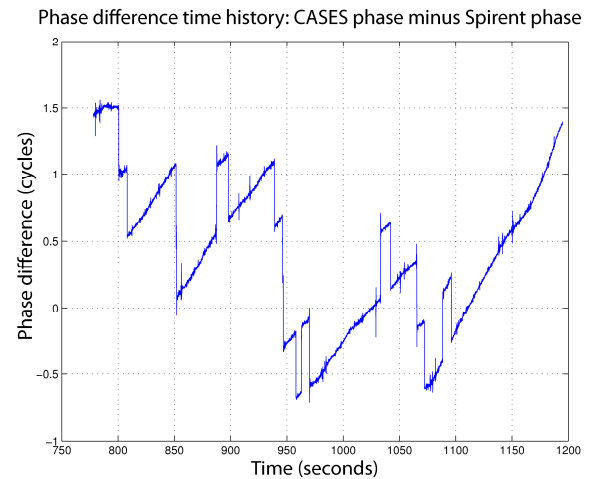

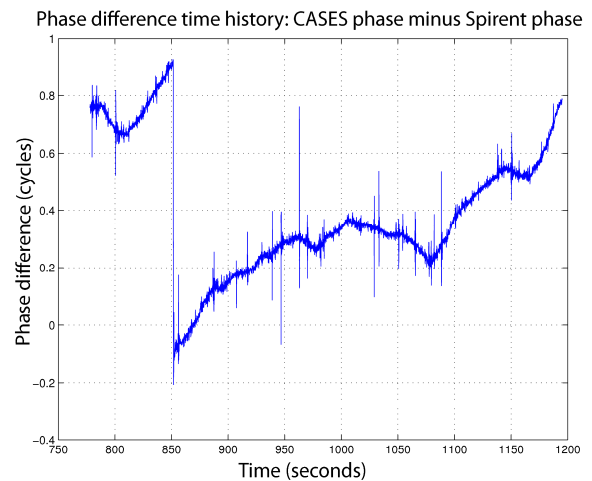*Fig. 9 Phase error without use of data bit prediction.*

Fig. 10 Phase error with data bit prediction.

The diagonal trend of the line sections is due to clock rate differences between the simulator and the receiver, and it should be noted that the vertical scales of the graphs differ in order to show as much detail as possible on each. Fig. 9 shows 16 half- or full-cycle slips. Fig. 10 shows only a single full cycle slip over the same period, thus it performs much better.

It should also be noted that while using the data bit prediction algorithm, only full cycle slips occur rather than half cycle slips, which are generally easier to remove in post-processing.

C. Comparison with a commercial scintillation monitor

CASES receivers were validated during a field campaign at the Jicamarca Radio Observatory near Lima, Peru in March, 2011. Six receivers were deployed in a small-baseline (~1 kM) array with the intent of observing scintillation and validating the ability of the receiver to operate while experiencing severe scintillation. Some observations recorded during this campaign have already been shown in Figs. 3, 4, and 6. One additional scintillation event is shown in Figs. 11 and 12. In Fig. 11, amplitude data from both CASES and a commercial scintillation monitor are shown in the top panel, with CASES in blue and the commercial receiver in red. Additionally, the bottom panel shows reported L1 C/A lock time for the commercial receiver. This plot illustrates that the commercial receiver lost lock several
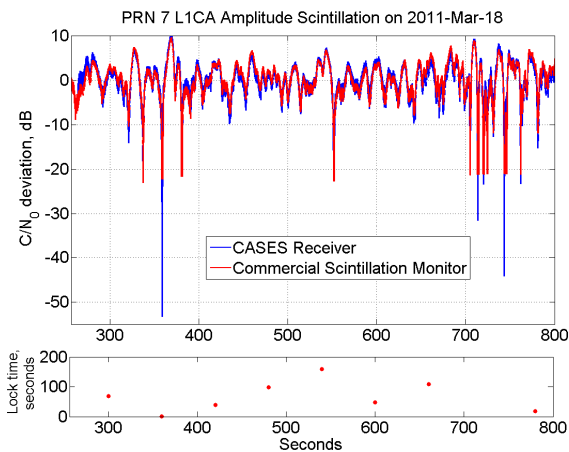

Fig. 11 Amplitude scintillation observed by CASES and a commercial scintillation monitor

times during the severe amplitude fades while CASES retained signal lock. S_4 during this period exceeded 0.9. A zoomed-in look at this plot between 700-770 seconds is shown in Fig. 12. These plots show that CASES is capable of tracking through even quite severe scintillation.
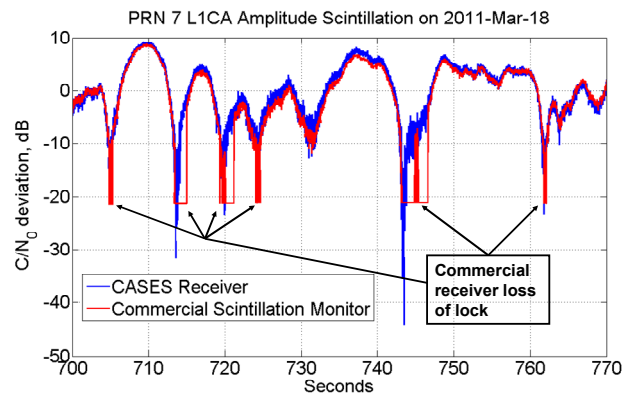

Fig. 12 Amplitude scintillation observed by CASES and a commercial scintillation monitor

VI. CONCLUSIONS

A software-defined dual-frequency GPS receiver has been designed for use as a space weather monitoring instrument. This software has been embedded in a flexible and capable hardware platform that allows remote monitoring, data logging, and reconfiguration. This receiver has implemented several novel software processing techniques that allow it to excel at monitoring space weather due to an advanced triggering technique, special data buffering, removal of local clock effects, and a data bit prediction algorithm that makes it particularly robust to ionospheric scintillation. This platform has been tested both in the field and the laboratory and shown to have marked advantages versus receivers lacking these features.

NOTES

This receiver is being commercialized by ASTRA LLC (www.astraspace.net) of Boulder, CO.

REFERENCES

[1] Crowley, G., Bust, G.S., Reynolds, A., Azeem, I., Wilder, R., O'Hanlon, B.W., Psiaki, M.L., Powell, S., Humphreys, T., and Bhatti, J., "CASES: A Novel Low-Cost Ground-based Dual-Frequency GPS Software Receiver and Space Weather Monitor," *Proceedings of the ION GNSS 2011*, Portland, OR, this issue.

[2] Lambert Wanninger, "Effects of the Equatorial Ionosphere on GPS," *GPS World,* July 1993 pp 48-54.

[3] Humphreys, T.E., Psiaki, M.L., Kintner, P.M., Jr., and Ledvina, B.M., "GNSS Receiver Implementation on a DSP: Status, Challenges, and Prospects," *Proceedings of the ION GNSS 2006*, Fort Worth, TX,

8

[4] O'Hanlon, B.W., Psiaki, M.L., Kintner, P.M., Jr., and Humphreys, T.E., "Development and Field Testing of a DSP-Based Dual-Frequency Software GPS Receiver," *Proceedings of the ION GNSS 2009*, Savannah GA.

[5] Van Dierendonck, A.J., "How GPS receiver Measure (or Should Measure) Ionospheric Scintillation and TEC and How GPS Receivers are Affected by the Ionosphere," *Proceedings of the 11th International Ionospheric Effects Symposium*, Alexandria, VA, 2005, pp 651-659.

[6] Humphreys, T.E., Psiaki, M.L., Kintner, P.M., and Ledvina, B.M., "GPS Carrier Tracking Loop Performance in the presence of ionospheric scintillations," *Proceedings of the ION GNSS 2005*, Long Beach, CA, pp 156-167.

[7] Skone, S., Knudsen, K., and de Jong, M., "Limitations in GPS Receiver Tracking Performance Under Ionospheric Scintillation Conditions," *Proceedings of the First COST Action 716 Workshop Towards Operational GPS Meteorology and the Second Network Workshop of the International GPS Service (IGS),* Vol. 26, pp 613-621.

[8] Rino, C.L., Gonzalez, V.H., and Hessing, A.R., "Coherence Bandwidth Loss in Transionospheric Radio Propagation," *Radio Science*. Vol. 16, No. 2, pp 245-255.

[9] Fremouw, E.J., Leadabrand, R.L., Livingston, R.C, Cousins, M.D., Rino, C.L., Fair, B.C., and Long, R.A., "Early Results from the DNA Wide-Band Satellite Experiment -- Complex Signal Scintillation," *Radio Science*, Vol. 13, No. 1, pp 167-187.

[10] Van Dierendonck, A.J., Klobuchar, J., and Hua, Q., "Ionospheric Scintillation Monitoring Using Commercial Single Frequency C/A Code Receivers," *Proceedings of ION GPS 1993*, Salt Lake City, UT, pp 1333-1342.

[11] Humphreys, T.E., Psiaki, M.L., Ledvina, B.M., Cerruti, A.P., and Kintner, P.M. Jr., "A data-driven test bed for evaluating GPS carrier tracking loops in ionospheric scintillation," *IEEE Transactions on Aerospace and Electronic Systems*, Vol. 46, No. 4, October 2010, pp 1609-1623.

[12] Beach, T.L., "Perils of the GPS Phase Scintillation Index (σ_φ)," *Radio Science*. Vol. 41, RS5S31.

[13] Humphreys, T.E., Psiaki, M.L., and Kintner, P.M. Jr., "Modeling the effects of ionospheric scintillation on GPS carrier phase tracking," *IEEE Transactions on Aerospace and Electronic Systems*, Vol. 46, No. 4, October 2010 pp 1624-1637.

[14] Simon, M.K., and Lindsey, W.C., "Optimum Performance of Suppressed Carrier receivers with Costas Loop Tracking," *IEEE Transactions on Communications*, Vol. 25, No. 2, February 1977, pp 215-227.

[15] Misra, P., and Enge, P., "Global Positioning System, Signals, Measurements, and Performance," Ganga-Jamuna Press, Lincoln MA, 2006.

[16] Van Dierendonck, A.J., "Global Positioning System: Theory and Applications, Chapter 8: GPS Receivers," American Institute of Aeronautics and Astronautics, Washington D.C., 1996 pp 329-407.

[17] Humphreys, T.E., Psiaki, M.L., Hinks, J.C., O'Hanlon, B., and Kintner, P.M. Jr., "Simulating Ionosphere-Induced Scintillation for Testing GPS Receiver Phase Tracking Loops," *IEEE Journal of Selected Topics in Signal Processing*, Vol. 3, No 4., August 2009